The juxtamembrane linker in neutral sphingomyelinase-2 functions as an intramolecular allosteric switch that activates the enzyme

Received for publication, December 23, 2018, and in revised form, March 8, 2019 Published, Papers in Press, March 19, 2019, DOI 10.1074/jbc.RA118.007288

Prajna Shanbhogue[‡§], Reece M. Hoffmann[¶], Michael V. Airola[‡], Rohan Maini[‡], David J. Hamelin[¶], Miguel Garcia-Diaz[‖], John E. Burke[¶], and Yusuf A. Hannun[‡§‖1]**

*From the Departments of [‡]Biochemistry and Cell Biology, **Medicine, and [‖]Pharmacological Sciences, Stony Brook University, Stony Brook, New York 11794, the [§]Stony Brook University Cancer Center, Stony Brook, New York 11794, and the [¶]Department of Biochemistry and Microbiology, University of Victoria, Victoria, British Columbia V8N 1A1, Canada*

Edited by George M. Carman

Neutral sphingomyelinase 2 (nSMase2) produces the bioactive lipid ceramide and has important roles in neurodegeneration, cancer, and exosome formation. Although nSMase2 has low basal activity, it is fully activated by phosphatidylserine (PS). Previous work showed that interdomain interactions within nSMase2 are needed for PS activation. Here, we use multiple approaches, including small angle X-ray scattering, hydrogen–deuterium exchange–MS, circular dichroism and thermal shift assays, and membrane yeast two-hybrid assays, to define the mechanism mediating this interdomain interactions within nSMase2. In contrast to what we previously assumed, we demonstrate that PS binding at the N-terminal and juxtamembrane regions of nSMase2 rather acts as a conformational switch leading to interdomain interactions that are critical to enzyme activation. Our work assigns a unique function for a class of linkers of lipid-activated, membrane-associated proteins. It indicates that the linker actively participates in the activation mechanism via intramolecular interactions, unlike the canonical linkers that typically aid protein dimerization or localization.

Ceramide is not only an integral part of cellular membranes but also an important bioactive lipid that regulates various signaling pathways pertaining to cell proliferation, apoptosis, differentiation, and various inter- and intracellular communication pathways (1–3). Accordingly, ceramide production plays an important role in cancer, as well as cardiovascular, neurodegenerative, pulmonary, and inflammatory conditions (4–10). Ceramide is produced through three major pathways: a *de novo* synthesis pathway catalyzed by ceramide synthases, a salvage pathway wherein sphingoid bases are recycled to make ceramide, and a hydrolytic pathway, predominantly catalyzed by sphingomyelinases (SMases).[2]

SMases are phosphodiesterases that generate ceramide by hydrolyzing sphingomyelin (SM) and releasing a phosphocholine moiety as byproduct. They are broadly classified, based on their pH optima, into acid sphingomyelinases, neutral sphingomyelinases (nSMases), and alkaline sphingomyelinases. nSMases are further classified into anionic phospholipid (APL)-independent nSMase1, APL-dependent nSMase2, a *Bovine* nSMase3, and a mitochondria-associated nSMase4. nSMase2 has been widely studied for its roles in cell growth, stress responses, and exosome release (11–13). Dysregulation in nSMase2 activity has been implicated in cancer, cardiovascular, and neurological conditions, such as Alzheimer's disease (14, 15), thus making it an important therapeutic target.

nSMase2 is most abundantly found in the plasma membrane and the Golgi, but it has also been studied in the context of endoplasmic reticulum stress and DNA damage response (7, 16, 17). Biochemical studies of nSMase2 have shown that its full activation requires Mg^{2+} and APLs such as PS and phosphatidic acid (PA). nSMase2 has an N-terminal domain (NTD) that aids in APL binding, followed by a cytoplasmic juxtamembrane region (JX), an insertion region, and a catalytic domain (CAT) (Fig. 1*A*). The NTD contains two hydrophobic segments, HS1 and HS2, that are important for APL-mediated allosteric activation of nSMase2. The first APL-binding site is between HS1 and HS2 on nSMase2, and the second APL-binding site includes a portion of the JX region (13, 18). The insertion region is presumed to regulate nSMase2 through its five phosphorylation sites and calcineurin-binding site (19); however, deletion of this region does not affect basal nSMase2 activity (20).

This work was supported by Grants R35 GM118128 (to Y. A. H.), a new investigator grant from the Canadian Institutes of Health Research; a Natural Sciences and Engineering Research Council of Canada Discovery Grant 2014-05218; and Canadian Institutes of Health Research Grants 148596 (to J. E. B.) and R35 GM128666 (to M. V. A.). The authors declare that they have no conflicts of interest with the contents of this article. The content is solely the responsibility of the authors and does not necessarily represent the official views of the National Institutes of Health.

This article contains Tables S1–S4 and Figs. S1–S4.

[1] To whom correspondence should be addressed. E-mail: yusuf.hannun@stonybrookmedicine.edu.

[2] The abbreviations used are: SMase, sphingomyelinase; nSMase2, neutral SMase-2; PS, phosphatidylserine; SAXS, small angle X-ray scattering; HDX-MS, hydrogen-deuterium exchange mass spectrometry; SM, sphingomyelin; APL, anionic phospholipid; PA, phosphatidic acid; NTD, N-terminal domain; JX, juxtamembrane region; CAT, catalytic domain; HS1, hydrophobic segment 1; HS2, hydrophobic segment 2; NTD-JX, construct containing N-terminal domain and juxtamembrane region; JX-CAT, construct containing juxtamembrane region and catalytic domain; β-gal, β-galactosidase; EV, empty vector; NUb, N-terminal end of ubiquitin; NUbI, isoleucine substituted at position 3 making NUb constitutively active; FL, full-length; HU, hydroxyurea; DOPC, 1,2-dioleoyl-*sn*-glycero-3-phosphocholine; DOPS, 1,2-dioleoyl-*sn*-glycero-3-phospho-L-serine; β-ME, β-mercaptoethanol; Aβ, amyloid β-peptide; OD, optical density.

© 2019 Shanbhogue et al. Published under exclusive license by The American Society for Biochemistry and Molecular Biology, Inc.

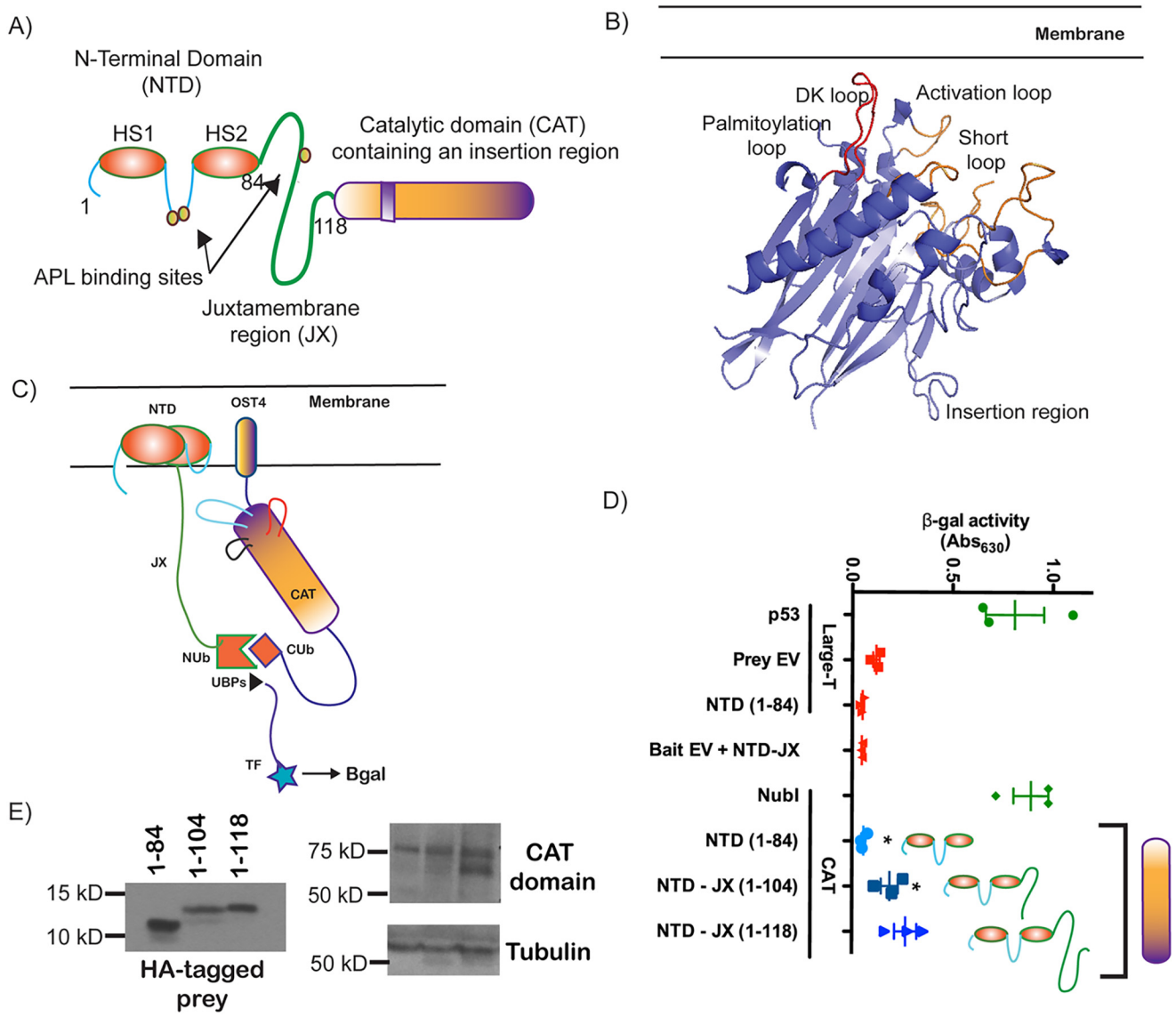

Figure 1. Domain architecture and structure of nSMase2. *A*, domain architecture of nSMase2. It has a membrane-inserted NTD containing two hydrophobic segments, HS1 and HS2 (shown in *orange*), that help in APL binding. This is followed by a cytoplasmic JX (shown as a *green line*), a catalytic domain (*CAT*, shown in *yellow* and *purple*), and an insertion region. *B*, X-ray crystallographic structure of the CAT domain of nSMase2. Of note are the various loops projecting from the membrane facing end of the domain–palmitoylation loop (containing two cysteine residues that are palmitoylated), a DK loop (previously shown to play a key role in substrate recognition and catalysis), a short loop, and an activation loop. *C*, schematic representation of the split ubiquitin membrane yeast two-hybrid system. The bait contains the CAT, which is tethered to the membrane through the OST4 membrane anchor and has the C terminus of ubiquitin (*CUb*) followed by transcription factors to signal β-galactosidase production. The prey contains the NTD or NTD-JX tethered to the NUb. *D*, relative β-gal activity. *Green shapes* indicate positive controls: p53, Large T, and NUbl (a self-activating ubiquitin). Negative controls in *red shapes* include prey EV and bait EV. The data represent means ± S.D. of $n = 3$. *E*, Western blots showing expression levels of prey and bait constructs. Tubulin is used as loading control.

The first crystal structure of the CAT domain of human nSMase2 was recently determined at 1.85 Å resolution, presumably in a low-activity state (Fig. 1*B*) (20). Additionally, a loop in the CAT called the "DK loop" was shown to play a role in activation of nSMase2 by acting as a gatekeeper loop (20). However, we did not understand how PS binding by the NTD and JX regions resulted in allosteric activation of the CAT. Here, we present extensive data to demonstrate that the JX region acts as a molecular scaffold, mediating a large conformational change upon PS binding and also effectively participating in activation of nSMase2 via a network of interdomain interactions essential to maintain the active conformation of nSMase2. Moreover, we also elucidate the importance of these interdomain interactions in nSMase2 function.

Results

The CAT domain of human nSMase2 interacts with the NTD through its JX region

Previous data on the mechanism of nSMase2 activation revealed that activation of this enzyme involves interaction of the CAT domain with the NTD (20). However, the molecular details of this interaction were not well-defined. To further characterize the mechanism of activation, a split ubiquitin membrane yeast two-hybrid system was developed with the CAT domain as bait and the NTD or NTD-JX domain as prey to determine the residues that play a role in this intramolecular interaction (Fig. 1*C*). This method relies on the fact that an interaction between bait and prey proteins results in reconsti-

tution of ubiquitin, which is further recognized by cytosolic deubiquitinases. This results in proteolytic release of a transcription factor (LexA-VP16) that facilitates β-gal production, which can then be measured as a readout of interdomain interactions (21). The well-established SV40 Large T antigen (as bait)–p53 (as prey) interaction was used as a positive control to test this system (Fig. 1*D*). Replacing either bait or prey with the corresponding empty vectors (pDHB1 or pPR3N) resulted in no β-gal production (Fig. 1*D*). Additional controls for validation of bait and prey were included to ensure elimination of false-positives. A self-inducing prey, NUbI was co-expressed with the CAT domain of nSMase2 as bait, resulting in a strong positive interaction. NTD-JX as prey was also tested against the bait vector pDHB1, resulting in no β-gal production. Expression of the constructs is shown in Fig. 1*E*. With these controls established, the results showed significant interaction between the NTD-JX (amino acids 1–104 and 1–118) and the CAT domains, as seen before (20). Importantly, the current data showed that deletion of the JX region led to a complete loss of interaction between the CAT domain and the membrane-inserted NTD (amino acids 1–84) despite higher expression of NTD (Fig. 1, *D* and *E*), indicating a necessary role for the JX region. The results suggest that the first 20 residues of the JX region (amino acids 85–104) are necessary for the interaction with the CAT domain to take place. Therefore, these results define a critical role for the JX region in the interaction with the catalytic domain.

Interdomain interactions occur through key amino acid residues in the JX region

To point out specific residues in the JX region that may be interacting with the CAT domain, a multiple sequence alignment of the JX region was performed. The alignment revealed that several amino acids were conserved across multiple species in the minimum sequence (residues 85–104) required for interactions between NTD-JX and CAT. Therefore, alanine scanning was performed across this conserved JX patch in the NTD-JX to define the residues that may play a role in interacting with the CAT domain (Fig. 2*A*). To rule out expression effects on interdomain interactions, Western blotting of these constructs is shown in Fig. 2*E*. Mutation of NTD-JX residues Leu-88, Gln-89, Pro-94, and Tyr-95 to alanine showed similar interaction strength as the WT NTD-JX, indicating that these residues do not play a role in interacting with CAT domain. Mutation of NTD-JX residues Arg-92–Arg-93 or Tyr-97 to alanine led to a significant decrease in interaction, suggesting that these residues play a role in interacting with the CAT domain. Interestingly, mutation of residues Trp-85 and Pro-87 to alanine increased the relative strength of interaction (Fig. 2*B*). We attributed this increase to reduced steric hindrance at these amino acid positions, aiding interdomain interactions. Removal of a bulky side chain in the Trp or any kinks that may be caused by the Pro possibly brought the cytoplasmic section of nSMase2 closer to the NTD, thus aiding stronger interactions. Together, these results indicate that residues Arg-92–Arg-93 and Tyr-97 in the JX region are important for interaction with the CAT domain.

Key residues in the CAT domain interact with the JX region

The membrane facing side of the CAT domain is most likely to participate in interdomain interactions with the JX domain because it too must lie close to the membrane. To define the interaction partners of the JX residues with the CAT domain, we performed an alanine scan of amino acids in four loops facing the membrane: the palmitoylation loop, DK loop, activation loop, and short loop (Fig. 2*C*). The orientation of the CAT domain in relation to the membrane was previously discussed by our group (20). Co-expression of NTD as prey and the CAT domain as bait was used as a negative control, and the interaction between NTD-JX as prey and CAT domain as bait was used as positive control. Mutation of residues in the activation loop (termed appropriately due to its active role in nSMase2 activation) of the CAT domain to alanine resulted in a decrease in interdomain interaction, suggesting residues N142AN143A and Leu-144 (despite its higher expression level) in this loop as the major interacting partners of the JX region (Fig. 2*D*). Mutations in residues Asn-428 and Asp-429 in the DK loop also resulted in a slight decrease in the relative strength of interdomain interactions. These data are consistent with the previously described model wherein a conformational change of this loop or "DK switch" needs to occur for activation of nSMase2. Mutations in the palmitoylation loop (L386AY387A and D388A V389A) and in the short loop (F400AK401A) did not show a difference in the relative strength of the interaction as compared with the WT NTD-JX construct and therefore do not appear to play a role in interactions between NTD-JX and CAT domains. Expression of the constructs is shown in Fig. 2*E*. These results identify residues N142AN143A and Leu-144 in the activation loop as important to mediate the interaction with the JX region.

The JX region acts as a bridge and mediates interactions with the NTD

A comparison of activity between the CAT, JX-CAT domains, and full-length (FL) nSMase2 constructs revealed that although tethering of the JX region to CAT is sufficient for activation by PS, the activity of the JX-CAT construct is only ~25% of the FL construct (Fig. 3*A*). Therefore, we hypothesized that the JX region may be mediating interactions between the NTD and CAT by also making important contacts with the NTD for maximal activation of the enzyme. To explore this, we again used the membrane split ubiquitin system, but in this case with NTD as prey and JX tethered to CAT (JX-CAT) as bait (Fig. 3*B*). Tethering JX to NTD (as NTD-JX) or to CAT (as JX-CAT) resulted in domain–domain interactions between NTD and CAT via the JX region. This suggests that the JX region acts as a bridge or a scaffold between the membrane-inserted NTD and the cytoplasmic CAT domains, making interactions with both domains.

The JX region interacts with the NTD through specific residues

To determine the specific amino acids that play a role in the JX-NTD interaction, point mutations of conserved residues in the JX region (Fig. 2*A*) were made in the JX-CAT construct and used as bait to probe against the prey, NTD. When vector pPR3N was used as prey and tested against JX-CAT as bait, no

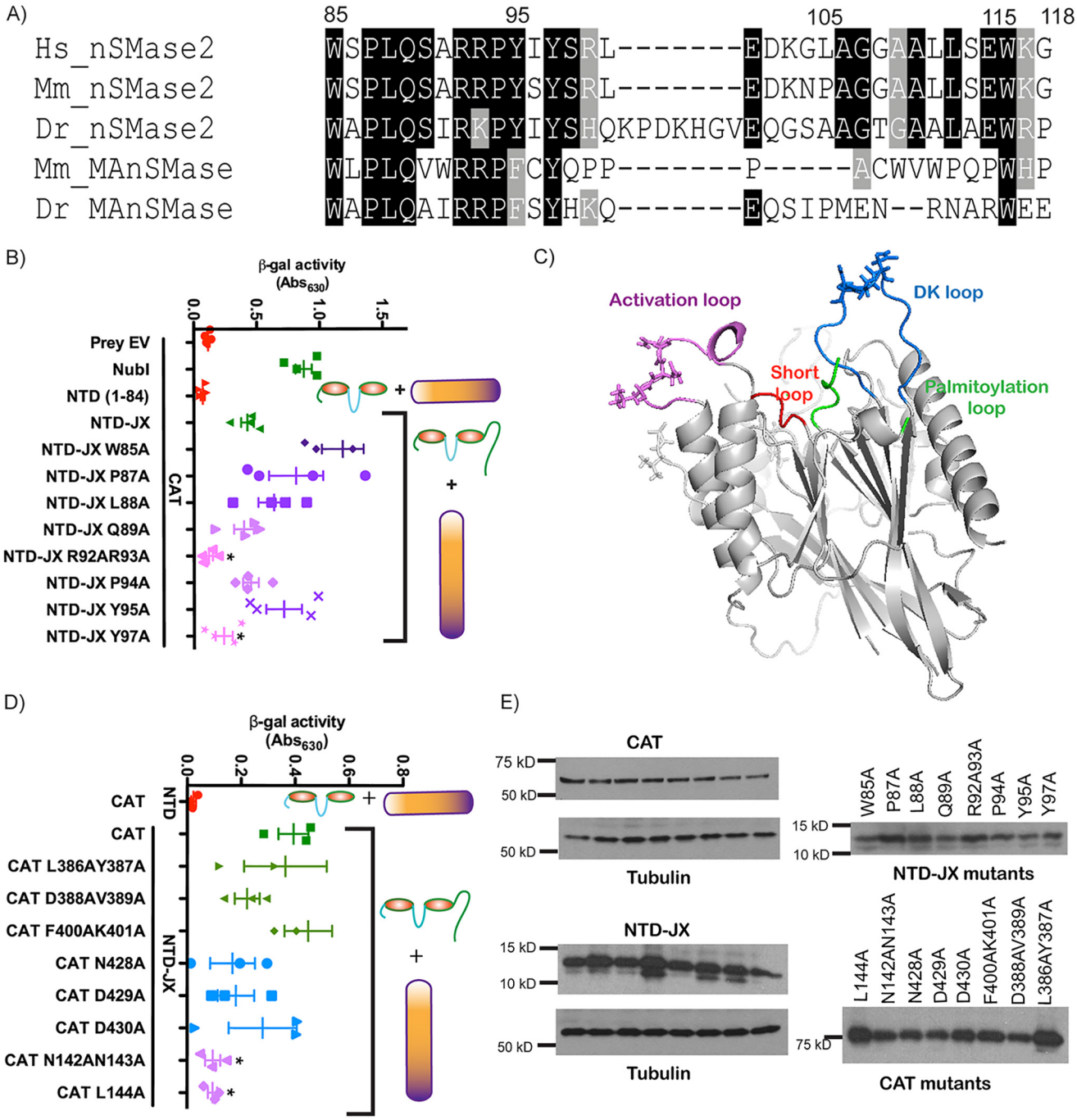

Figure 2. Interdomain interactions between NTD-JX and CAT occur via specific residues. *A*, multiple sequence alignment of the JX region indicating conserved residues across *Homo sapiens* (*Hs*), *Mus musculus* (*Mm*), and *Danio rerio* (*Dr*), and *M. musculus* mitochondria-associated SMase and *D. rerio* mitochondria-associated SMase. *B*, membrane yeast two-hybrid readout of β-gal activity with NTD or NTD-JX as prey and CAT as bait. *Green shapes* indicate positive controls (NUbI and WT NTD-JX), and *red shapes* indicate negative controls (prey EV and NTD WT). The data represent means ± S.D. of $n = 3$. *Asterisks* indicate statistically significant decrease in readout as tested by a Student's *t* test between positive control NUbI and individual mutations. *C*, structure of the CAT domain of nSMase2 with various loops that project toward the membrane. Activation loop mutations are highlighted in *purple*, DK loop mutations are in *blue*, and the palmitoylation loop is in *green*. *D*, membrane yeast two-hybrid readout of β-gal activity with NTD or NTD-JX as prey and CAT as bait. *Dark green shapes* indicate positive control (WT CAT), and *red shapes* indicate negative control (WT NTD). *Light green shapes* indicate mutations in palmitoylation loop, *blue shapes* highlight mutations in DK loop, and *purple shapes* show mutations of the activation loop. The data represent means ± S.D. of $n = 3$. *Asterisks* indicate statistically significant decrease in readout as tested by a Student's *t* test between positive control NUbI and individual mutations. *E*, Western blots indicating expression levels of prey and bait constructs. Tubulin is used as loading control.

interaction was seen, thus ensuring no false positives. The positive control for the system was the self-inducing prey, NUbI, with JX-CAT as bait that resulted in a strong increase in β-gal activity. When JX-CAT WT was used as bait against NTD as prey, as expected, there was an increase in β-gal activity, which was abolished when JX-CAT was replaced with CAT as bait (Fig. 3*C*). Mutation of JX residues Leu-88, Gln-89, Pro-94, and Tyr-95 to alanine did not show a significant decrease in β-gal activity, thus indicating that they are not involved in interactions between NTD and JX-CAT. However, mutation of resi-

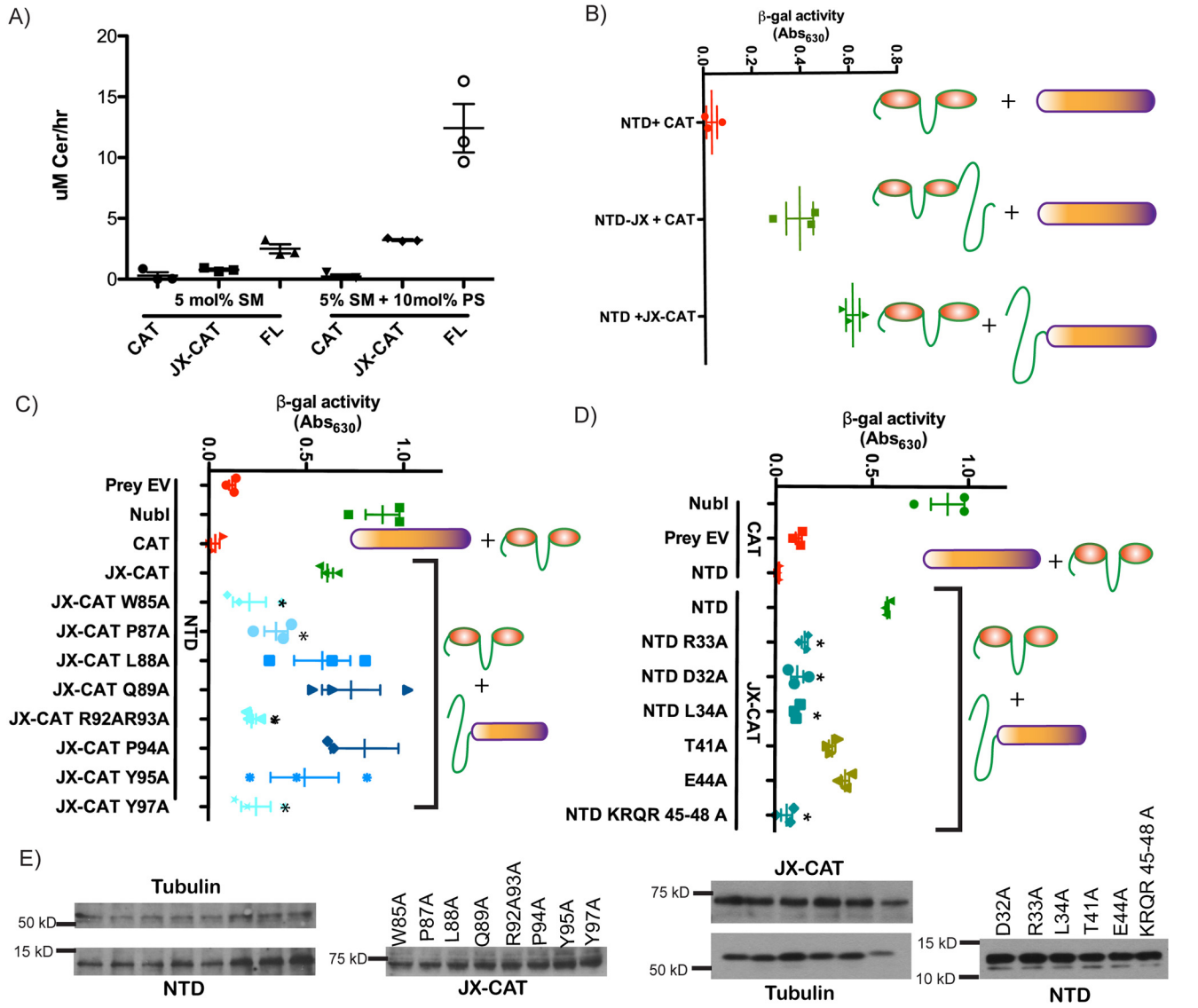

Figure 3. Interdomain interactions between NTD and JX-CAT occur via specific residues. *A*, activity assay comparisons between CAT domain, JX-CAT domain, and FL nSMase2 with and without the presence of PS. *B*, membrane yeast two-hybrid readout of β-gal activity when JX region is tethered to NTD (as prey, NTDJ-X) or to CAT (as bait, JX-CAT). The data represent means ± S.D. of $n = 3$. *C*, membrane yeast two-hybrid readout of β-gal activity with NTD as prey and CAT or JX-CAT as bait. *Green shapes* indicate positive controls (NUbI and WT JX-CAT), and *red shapes* indicate negative controls (prey EV and CAT WT). The data represent means ± S.D. of $n = 3$. *Asterisks* indicate statistically significant decrease in readout as tested by a Student's *t* test between positive control NUbI and individual mutations. *D*, membrane yeast two-hybrid readout of β-gal activity with NTD as prey and CAT or JX-CAT as bait. The *dark green shapes* indicates positive control (WT JX-CAT), and *red shapes* indicates negative control (WT CAT). *Light green shapes* indicate mutations in NTD. The data represent means ± S.D. of $n = 3$. *Asterisks* indicate statistically significant decrease in readout as tested by a Student's *t* test between positive control NUbI and individual mutations. *E*, Western blots showing expression levels of prey and bait constructs. Tubulin is used as loading control.

dues Trp-85, Pro-87, Arg-92–Arg-93, and Tyr-97 resulted in a significant decrease in β-gal activity, thus indicating that they play a role in interacting with the NTD (Fig. 3*C*). Interestingly, Arg-92 and Arg-93 were important for both sets of interactions (JX with NTD and JX with CAT). From previous studies, we know that these two arginines play a role in PS binding (18). Therefore, this suggests that domain–domain interactions might be occurring as a consequence of PS binding. Expression levels of constructs do not contribute to differences in interdomain interactions as depicted in Fig. 3*E*. Therefore, these results show that specific amino acid residues in the JX region play a role in interacting with the membrane-inserted NTD.

Key residues in the NTD play a role in interdomain interactions

To determine the amino acids in the NTD that play a role in interacting with JX-CAT, point mutations in the conserved amino acid residues in the region between the two hydrophobic segments were made, including amino acids previously identified to be important for PS binding. This comes from a previous topological study of nSMase2 (22). Again, NUbI (prey)–CAT (bait) or NUbI (prey)–JX-CAT (bait) pairs were used as positive controls, and EV or NTD against CAT were used as negative controls. Conserved residues Thr-41 and Glu-44 showed very little change in β-gal activity, thus indicating that they play no role in interacting with the cytoplasmic section of nSMase2

(Fig. 3*D*). Residues Asp-32 and Leu-34 showed a decrease in β-gal activity. Amino acids previously recognized as important for PS activation of nSMase2, Arg-33, and the cationic patch KRQR (residues 45–48) (18) showed a significant decrease in β-gal activity (Fig. 3*D*). Expression levels of constructs are shown in Fig. 3*E*. Taken together, these results indicate that residues Asp-32 and Leu-34 in addition to PS-binding residues (Arg-33 and Lys-45–Arg-46–Gln-47–Arg-48) are involved in domain–domain interactions with the CAT.

Mutation of key JX residues that play a role in interdomain interactions reduce nSMase2 activity

To determine whether a loss of interaction between the NTD and CAT domains via the JX region indeed leads to a loss of nSMase2 activation, the effects of JX point mutations W85A, Y97A, R92AR93A; CAT domain mutations N142A, N143A, and L144A (in the activation loop); and NTD mutations D32A, R33A, L34A, and KRQR 45–48A in full-length nSMase2 were tested. The activity assay was performed by quantifying the hydrolysis of ^{14}C-labeled SM in mixed micelles ("Experimental procedures"). JX mutations W85A and Y97A drastically reduced the V_{max} by ~85%, whereas mutating residues Arg-92 and Arg-93 reduced the V_{max} by 30% (Fig. 4*A*). The CAT activation loop residues, N142A, N143A, and L144A also showed a decrease in V_{max} of ~80% (Fig. 4*A*). NTD mutations D32A and Leu-34 showed a complete loss of nSMase2 activity, and as previously shown, residues R33A and the cationic patch residues (KRQR 45–48) showed complete reduction in nSMase2 activity (Fig. 4*A*) (18). Mutating conserved residue Phe-400 did not result in a significant decrease in activity as compared with WT nSMase2, thus indicating that the loss of nSMase2 activity is due to a loss in interdomain interactions (Fig. 4*A*). To ensure that the loss of activity of nSMase2 is not due to loss of protein fold, we ran nSMase WT and nSMase2 mutant (containing all mutations involved in interdomain interaction) constructs on Phyre2 application (23). Comparison of WT and mutant nSMase2 constructs revealed no changes in secondary structure elements in mutated regions (Figs. S1 and S2). To confirm these results experimentally, we performed CD of CAT WT and JX-CAT WT with some representative mutations (CAT D430A, CAT N142AN143A, CAT L144A, JX-CAT W85A, JX-CAT R92AR93A, and JX-CAT Y97A). The spectra of CAT domain constructs look similar to those of previously published bacterial sphingomyelinases (24). No major changes in spectra were observed between WT and mutant constructs (Fig. S3).

Furthermore, we checked the thermal stability of CAT WT and JX-CAT WT with some representative mutations (CAT D430A, CAT N142AN143A, CAT L144A, JX-CAT W85A, JX-CAT R92AR93A, and JX-CAT Y97A) from the yeast two-hybrid screen using SYPRO orange dye with a temperature gradient from 25 to 95 °C. No significant changes in melting temperatures were observed between WT and mutational constructs (Fig. S4). These results indicated that the loss in nSMase2 activity in these mutant constructs were not due to a loss of secondary structural elements but could be due to a loss of interdomain interactions.

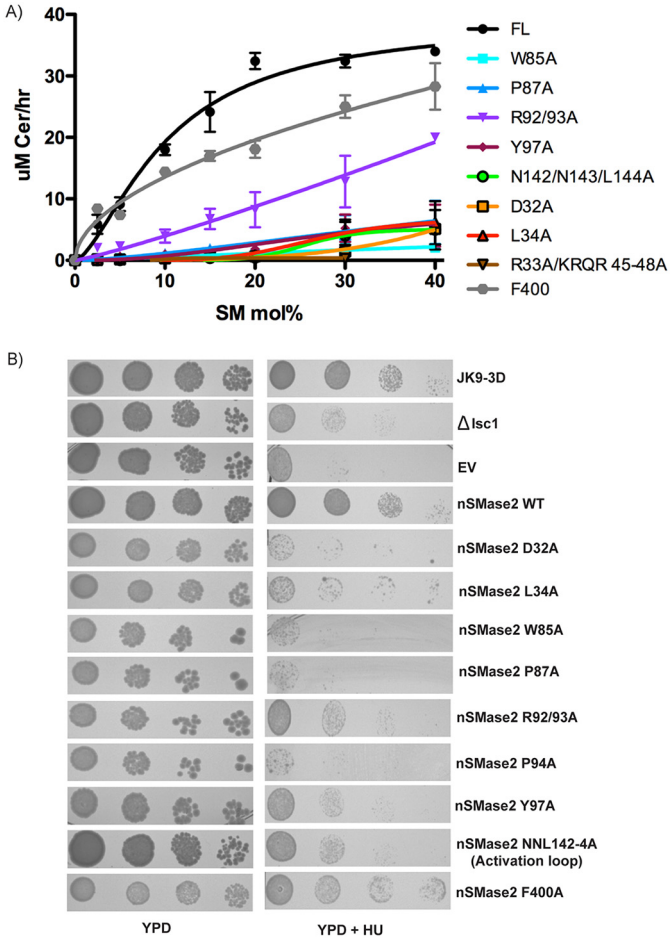

Figure 4. Interdomain interactions are required for activation of nSMase2. *A*, mutation of amino acids important for interdomain interactions eliminates activation of nSMase2 by PS. The data represent means ± S.D. of $n = 3$. *B*, interdomain interactions are necessary for nSMase2 function. Serial dilutions of overexpression constructs of full-length nSMase2 and nSMase2 mutations important for interdomain interactions in ΔIsc1 cells showing protection from HU.

Interdomain interactions are required for protection of Saccharomyces cerevisiae from hydroxyurea

To establish whether a loss of allosteric activation of nSMase2 via the JX region affects its function in cells, the sensitivity of the JK9-3d yeast strain to the genotoxic agent hydroxyurea (HU) was tested. As previously established, the JK9-3d strain lacking the yeast homolog of nSMase2 (Isc1) showed a clear sensitivity to HU. This phenotype was rescued with overexpression of human WT nSMase2 in these cells (Fig. 4*B*). Furthermore, when human nSMase2 was overexpressed with mutations relating to interdomain interactions such as Trp-85, R92AR93A, and Tyr-97 in the JX region, activation loop mutations in the CAT domain such as N142A, N143A, and L144A, or NTD mutations such as D32A, R33A, L34A, and KRQR 45–48A, a decrease in protection from HU was observed (Fig. 4*B*). On the other hand, mutating conserved residue Phe-400, which did not affect nSMase2 activity, yielded comparable growth to that of WT. Thus, the results indicate that protection from growth arrest is a result of nSMase2 activity, which in turn depends on interdomain interactions. Hence, these results establish that interdomain interactions are necessary for nSMase2 activation and play a vital role in its cellular function.

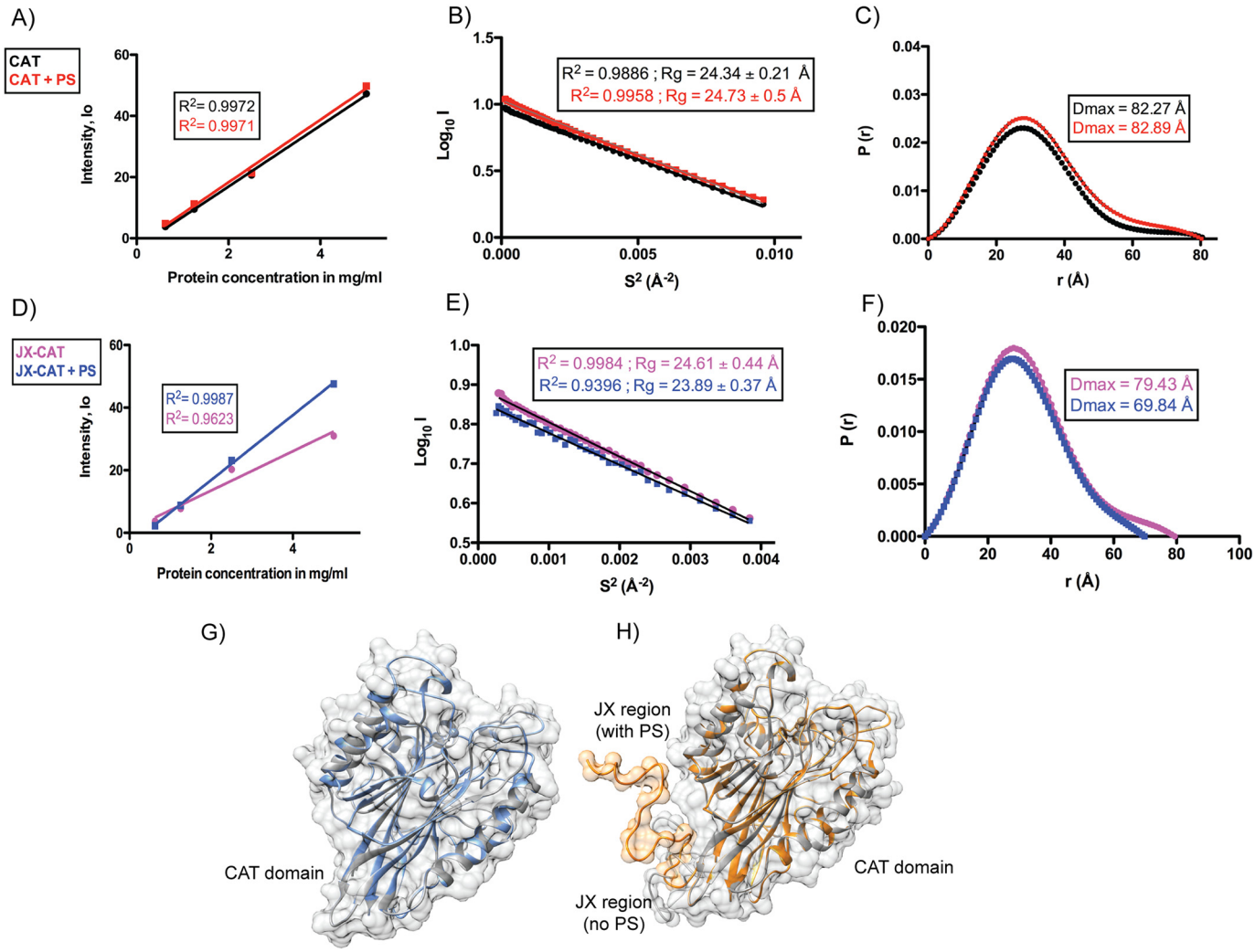

Figure 5. SAXS parameters for data validation and interpretation. *A*, I_0 *versus* protein concentration of nSMase2 CAT domain with and without PS. *B*, Guinier plot of nSMase2 CAT domain with and without PS. *C*, distance distribution function *P*(*r*) *versus* radius, *r*, for nSMase2 CAT domain with and without PS. *D*, I_0 *versus* protein concentration of nSMase2 JX-CAT domain with and without PS. *E*, Guinier plot of nSMase2 JX-CAT domain with and without PS. *F*, distance distribution function *P*(*r*) *versus* radius, *r*, for nSMase2 JX-CAT domain with and without PS. *G*, SAXS reconstruction of CAT domain in the presence and absence of PS. *H*, SAXS reconstruction of JX-CAT domain in the presence and absence of PS.

PS binding causes a conformational change in the cytoplasmic portion of nSMase2

Loss of interdomain interactions as a result of mutations in APL-binding residues posed the question of whether the PS binding induces these interdomain interactions or whether these domain–domain interactions primed nSMase2 for APL binding. To this end, first, we studied whether binding of PS by nSMase2 resulted in a conformational change in the enzyme. SAXS measurements were carried out using purified CAT and JX-CAT constructs in the presence or absence of PS. Plots of intensity at zero scattering angle, I_0, *versus* protein concentration for CAT and JX-CAT with and without PS indicated that all samples were monodisperse and suitable for SAXS analyses (Fig. 5, *A* and *D*). Guinier analysis and pair wise distribution, *P*(*r*), were calculated and plotted in Fig. 5, *B* and *C*, for CAT (with and without PS). Comparison of Guinier plots for CAT in the presence or absence of PS resulted in an overlap of the plot with little to no changes in the radius of gyration, R_g (Fig. 5*B*). The *P*(*r*) function for CAT in the presence or absence of PS also resulted in an overlap of plots with little to no changes in the protein radius, D_{max}, indicating that binding of PS to CAT results in no significant conformational changes (Fig. 5*C*). On the other hand, comparison of Guinier plots for JX-CAT in the presence or absence of PS resulted in a difference of 0.89 Å in R_g (Fig. 5*E*). The *P*(*r*) plot for JX-CAT in the presence or absence of PS also showed a 9.59 Å difference (~12% decrease) in D_{max} (Fig. 5*F*). SAXS reconstructions of CAT and JX-CAT constructs in the presence or absence of PS were performed using CORAL program in the ATSAS package (Fig. 5, *G* and *H*). The results from these analyses are provided in Table 1, which show that PS binding of JX-CAT results in a significant conformational change but that this conformational change is not observed in the CAT construct and thus seems dependent on the nSMase2 JX region.

The JX region does not increase HDX protection at the activation loop in the absence of PS

An independent and blinded study using hydrogen–deuterium exchange (HDX)–MS was used to probe the inter-

Table 1
SAXS parameters for data validation and interpretation

Parameters	CAT		JX-CAT	
	No PS	With PS	No PS	With PS
R_g Guinier plot (Å)	24.34 ± 0.21	24.73 ± 0.5	24.61 ± 0.44	23.89 ± 0.37
$P(r)$ (Å)	24.89	24.8	24.57	23.68
D_{max} (Å)	82.27	82.89	79.43	69.84
Goodness of fit, R^2	0.9886	0.9958	0.9984	0.9396

action of the CAT domain with the JX region. Here, the rate of exchange of amide hydrogens from the protein backbone with the solvent is measured as a means to determine protein secondary structure and conformational dynamics. The CAT and JX-CAT constructs were individually purified and allowed to undergo deuterium exchange at multiple different exposure times (3, 30, and 300 s) in their apo states at a final concentration of 400 nM. Deuterium incorporation is analyzed through the digestion of the proteins into peptides, followed by separation and mass analysis. Deuteration states for all analyzed peptides are provided in Tables S1 and S2.

Comparing the CAT and JX-CAT constructs revealed that the presence of the JX region caused an overall protection in the cytoplasmic face of the CAT domain. Peptides that only show protection at early time points (amino acids 383–387 and 385–391) are indicative of a weakly protected amide (highly dynamic secondary structure) that becomes protected in the JX-CAT construct; for peptides with differences mainly at the middle time points (amino acids 611–622), these are indicative of amides with medium levels of protection (more stable secondary structure) being protected, and finally peptides with divergence at late time points is indicative of strongly protected amides (very stable secondary structure) being protected (amino acids 440–455, 618–626, and 647–651) (Fig. 6, *A* and *B*). This indicates that the JX region is a highly dynamic, flexible linker that wraps around the cytoplasmic end of CAT domain in the absence of lipids and the NTD (Fig. 6, *A* and *B*).

Conformational change upon PS binding leads to interdomain interactions

To characterize the conformational changes observed by SAXS, we performed HDX-MS with the JX-CAT construct in the presence or absence of liposomes containing PS. nSMase2 JX-CAT constructs were incubated in the presence and absence of liposomes containing 30% SM, 30% DOPC, 30% DOPS, and 10% cholesterol. Membrane binding can frequently lead to protein instability over time and lead to aggregation issues. Therefore, HDX experiments were carried out using standard method for membrane proteins at three time points in triplicate (3, 30, and 300 s) for both conditions. JX-CAT was stable at all three time points. All identified peptides and their deuteration rates are tabulated in Tables S3 and S4.

In the presence of liposomes containing DOPS, decreased exchange rates were observed throughout the catalytic domain of nSMase2 JX-CAT. The largest change in deuteration (over 10%) in the CAT domain was observed in the activation loop (residues 139–145 and 145–149), suggesting that it could be participating in interdomain interactions or interacting with the lipid substrate. However, previous work from our group showed that nSMase2 lacking the NTD-JX region does not bind membranes containing DOPS (18). Moreover, our SAXS data (above) also shows no conformational changes in CAT in the presence of PS. Therefore, this protection of activation loop residues is most likely due to interdomain interactions. The palmitoylation loop (residues 552–557) also showed decreases in exchange rates >10%. The regions 170–350 and 486–500 showed also showed a 7–10% decrease in exchange (7–10%) (Fig. 7, *A* and *B*). In summary, these results show that the interaction with DOPS-containing membranes leads to conformational changes mediated through the JX region, thus positioning nSMase2 to make important interactions with the activation loop of the CAT domain.

Discussion

nSMase2 is emerging as a complex enzyme because it is regulated at multiple levels through layers of modular switches embedded into its structure. It has two membrane insertion domains, two palmitoylation clusters, a DK loop that acts as an autoinhibitory switch, an insertion region that controls post-translational modifications and protein–protein interactions via a calcineurin binding region, and requirement of anionic lipids and magnesium for full activation. Detailed biochemical and biophysical studies over the last decade have provided important information on the architecture and mechanism of nSMase2 CAT activation in generating ceramide. However, our understanding of the PS-mediated allosteric activation mechanism of nSMase2 still lags behind. In this study, the results show that the JX region of nSMase2, which links the NTD and the CAT, plays a critical role in allosteric activation of the CAT domain.

Our current data suggest that the 32-amino acid-long JX region is not merely a linker connecting the two major domains (NTD and CAT) of nSMase2 but is also a key player in inducing a conformational change upon PS binding and that it participates actively in interdomain interactions that are required for activation of nSMase2 (Fig. 8). The results show that specific amino acid residues in the JX region, Arg-92, Arg-93, and Tyr-97 are critical for interdomain interactions with the CAT domain. The results further provide evidence that the activation loop in the CAT domain drives nSMase2 activity by making specific intramolecular interactions with the JX region. The JX region also mediates interactions with the NTD via residues Trp-85, Pro-87, Arg-92, and Arg-93. Residues Asp-32, Arg-33, and Leu-34 and the cationic patch KRQR 45–48 in the NTD are shown to play a role in interacting with the JX region. Burial of these NTD charged residues in the membrane would be energetically costly, so they likely project into the polar environment, and interaction with residues in the cytoplasmic segment of nSMase2 would not only seem thermodynamically efficient but may also help stabilize nSMase2 during SM hydrolysis. These results clearly indicate that the JX domain actively interacts with both the CAT and the NTD and functions as a critical intermediate in the allosteric activation of the enzyme.

Importantly, Arg-92 and Arg-93 were found to participate in both interactions of the JX with CAT and with NTD. These residues were previously shown to be important for PS binding (18). Therefore, one plausible mechanism is that these two res-

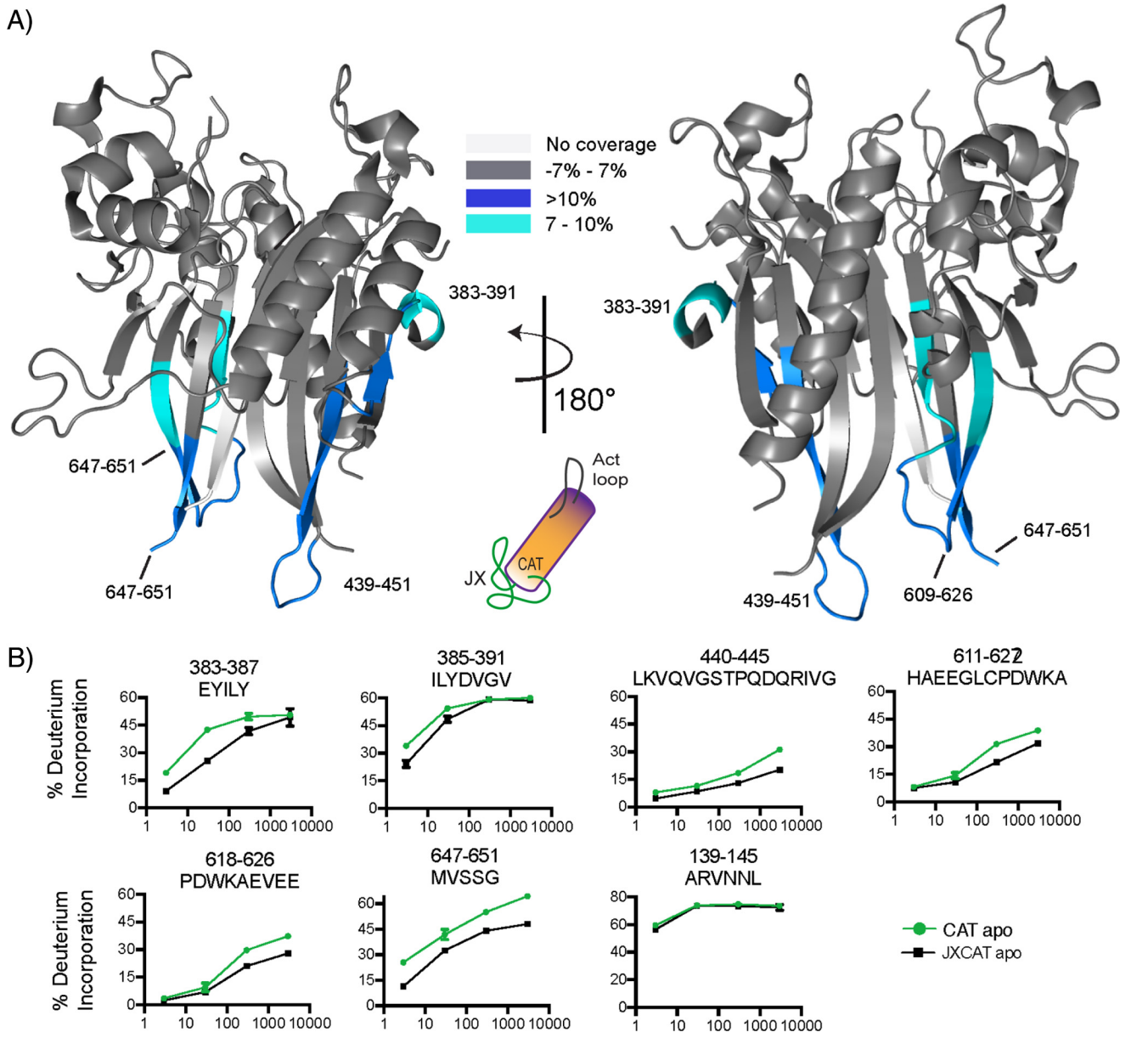

Figure 6. HDX-MS analysis for CAT *versus* JX-CAT. *A*, peptides in the CAT domain of nSMase2 that showed deuterium exchange differences greater than 7% and 0.4 Da when in the presence of the JX region are mapped onto a modeled structure of nSMase2's CAT domain (Protein Data Bank code 5UVG). Peptides showing less than 7% change in exchange rate are shown in *gray*, peptides showing a difference in exchange rate between 7 and 10% are shown in *light blue*, and peptides showing exchange rate differences over 10% are shown in *dark blue*. *B*, time course of deuterium incorporation for peptides in the nSMase2 CAT domain showing differences in percentage of deuteration between the shown conditions (error shown as S.D., $n = 3$). All mentioned peptides showed a decrease in exchange greater than 4 Da, as well as a paired *t* test value of $p < 0.05$.

idues are, at least partly, required for PS binding and therefore are important to transmit the allosteric interactions between the domains. It is to be noted that the requirements for the presence of PS could not be addressed using the yeast two-hybrid because PS is constitutively present in the system, and several attempts to create yeast NMY51 strains with CHO1 (gene that encodes for PS synthase) deletion were unsuccessful.

Therefore, the important question of whether these interdomain interactions occur as a result of PS binding or whether their "pre-existing" interactions allow PS binding was tested in a 2-fold manner. First, SAXS analyses on JX-CAT in the presence and absence of PS revealed that a conformational change occurs when JX-CAT binds PS. The reduction of D_{max} in the presence of PS suggests that the JX region might undergo a structural rearrangement possibly from an unstructured peptide to an α-helical or coil conformation, thus shortening the distance between CAT and the NTD. These results were further confirmed in a blinded and independent study using HDX-MS, wherein the rate of exchange of amide hydrogens from the protein backbone showed that the activation loop was protected only in the presence of PS. These results suggest that the binding to PS acts as a conformational trigger via the JX region, positioning the catalytic domain in an orientation that facilitates interdomain interactions. This structural rearrangement is also responsible for uncoupling of the DK switch, previously found to act as an autoinhibitory loop in the catalytic domain.

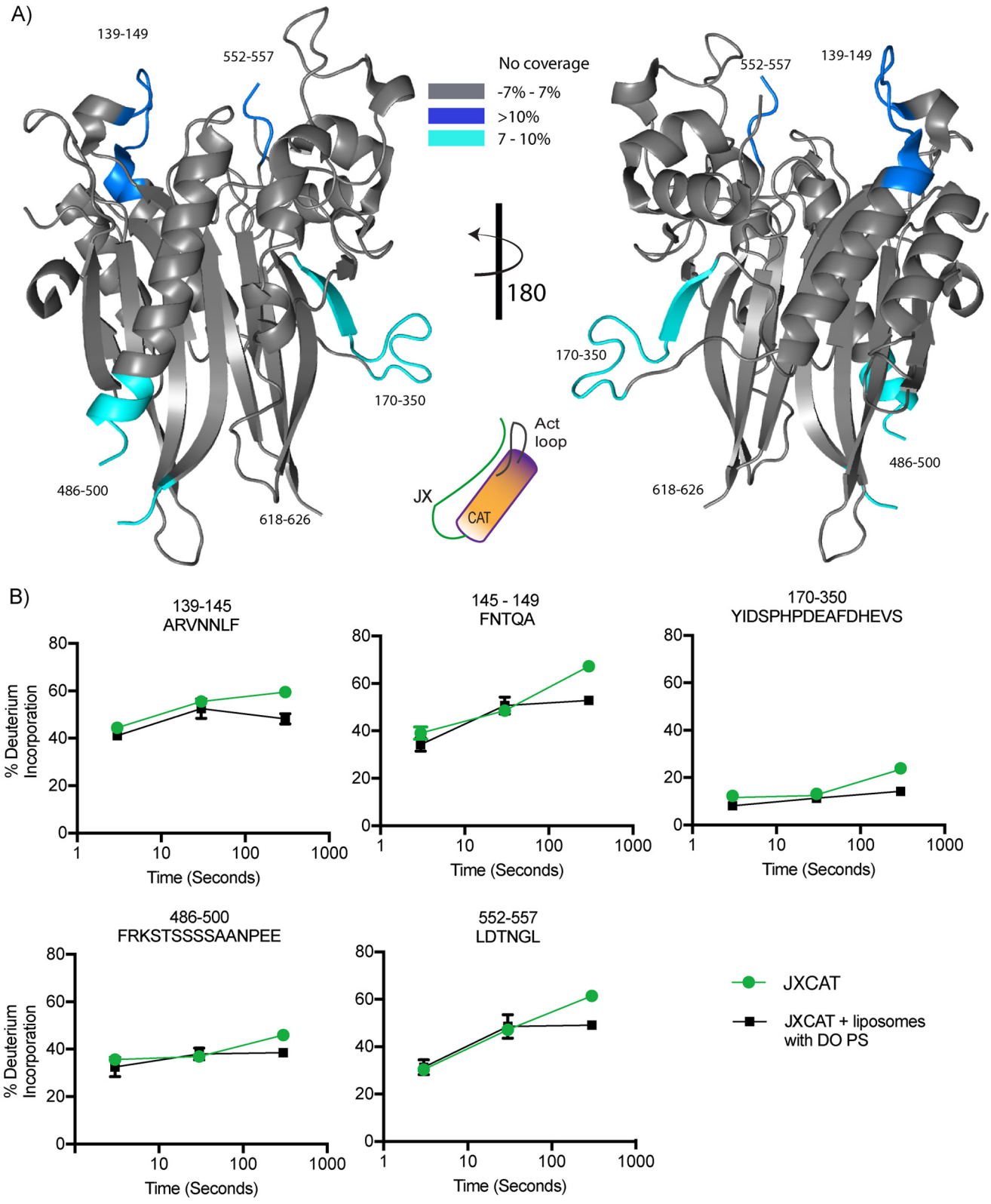

Figure 7. HDX-MS analysis for JX-CAT with and without PS. *A*, peptides in the JX-CAT domain of nSMase2 that showed deuterium exchange differences greater than 7% and 0.4 Da when in the presence of DOPS liposomes are mapped onto a modeled structure of nSMase2's CAT domain (Protein Data Bank code 5UVG). Peptides showing less than 7% change in exchange rate are shown in *gray*, peptides showing a difference in exchange rate between 7 and 10% are shown in *light blue*, and peptides showing exchange rate differences over 10% are shown in *dark blue*. Peptides showing increase in HDX exchange are shown in *orange*. *B*, time course of deuterium incorporation for peptides in the nSMase2 JX-CAT domain showing differences in percentage of deuteration between the shown conditions (error shown as S.D., $n = 3$). All mentioned peptides showed a decrease in exchange greater than 4 Da, as well as a paired *t* test value of $p < 0.05$.

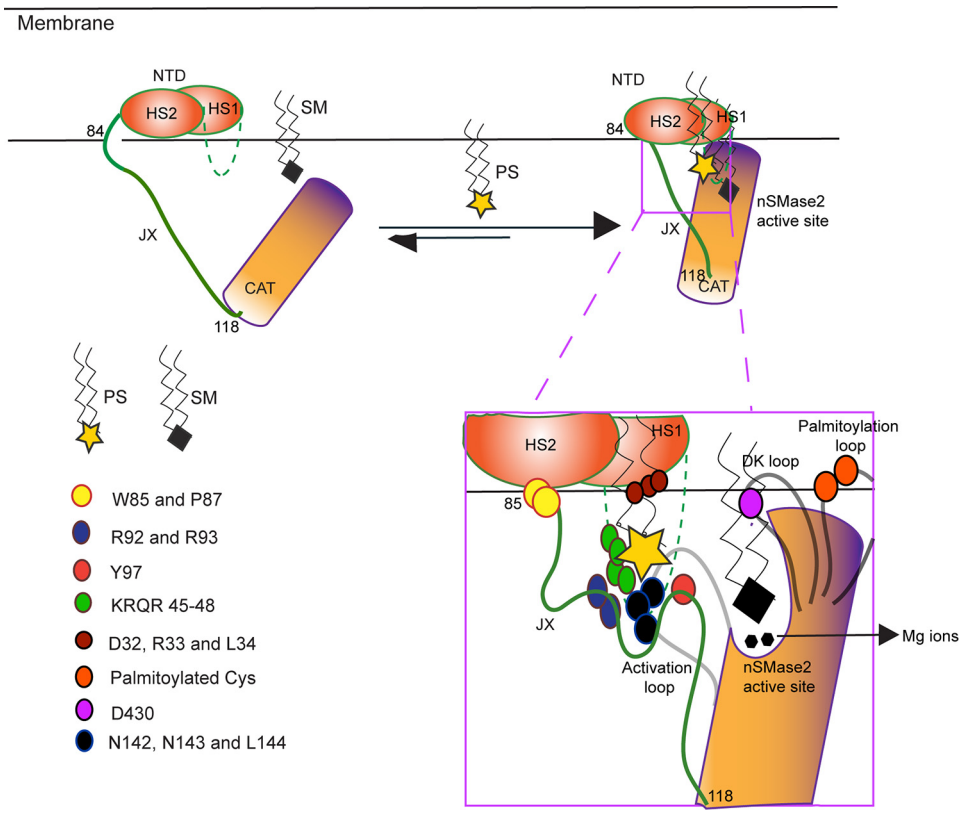

Figure 8. Model for nSMase2 activation. PS binding of nSMase2 causes a conformational change leading to interdomain interactions via the JX region, thus positioning the catalytic domain in the active conformation. The JX region acts as a scaffold facilitating PS and interdomain interactions, as shown in the *inset*. This suggests the mechanism of nSMase2 activation by PS.

The results also demonstrate that this network of interdomain interactions between NTD and CAT via JX region is important for nSMase2 function *in vitro* and in cells. First, the loss of the specific interdomain interactions led to a loss in enzyme activation. Second, the data also revealed a functional role for these interdomain interactions in cells. Here, the growth defect caused by HU in *S. cerevisiae* deleted in Isc1, the yeast homolog of nSMase2, could be overcome by WT nSMase2 but not by mutants in the critical residues required for these interactions. Therefore, interdomain interactions between NTD and CAT domain mediated by the JX region as a consequence of PS binding are required for nSMase2 activation and function.

Although no structures of the NTD have been reported, our findings support a PS-mediated stepwise allosteric activation model for regulation of nSMase2. nSMase2 not bound to PS represents an inactive or autoinhibited configuration of the enzyme wherein the DK loop occludes the active site of the enzyme (20). Upon binding to PS, for example in membrane microdomains with high localized PS concentrations such as the inner leaflet of the plasma membrane, a conformational change mediated through the JX region positions the CAT domain in its active conformation. This facilitates a network of intricate interactions between the NTD and the CAT domain that further help shift the equilibrium toward the active conformation of the enzyme, thus leading to SM hydrolysis and localized ceramide production (Fig. 8). Other factors that affect nSMase2 activity are pH, presence of Mg^{2+}, oxidation, and phosphorylation status of the enzyme. However, we believe that pH, Mg^{2+}, and oxidation status of nSMase2 affect enzyme activation through mechanisms that directly affect the charge status in the active pocket, thus disrupting acid–base catalytic mechanism rather than impact the allosteric activation mechanism we describe in this study. Furthermore, previous work on nSMase2 showed that deletion of region harboring the five known phosphorylation sites did not affect the interdomain interactions between the NTD and CAT domains (20).

Thus, we propose a dual role for the JX region: 1) in sensing changes in upstream signals or membrane by interacting with PS and 2) in rewiring the electrostatic circuitry of NTD-CAT interactions by adopting an active conformation, thus overcoming the DK checkpoint and leading to ceramide production. This forms the basis of our model for how an activation signal in the membrane is transduced across to the cytoplasm, leading to an amplification in ceramide production (Fig. 8). Such focused production of ceramide might be important in its function as a bioactive molecule responding to specific cellular signals such as tumor necrosis factor-α or $A\beta_{1-42}$, thus mediating a variety of cell signaling pathways such as inflammation and exosome formation (25, 26).

Although PS just forms ~3–10% of cell membrane, several studies have looked at the effects of PS concentration in various cellular membranes. Yeast that are deficient in PS synthase gene (cho1) showed defective vacuolar acidification and aberrant endocytic pathways (27). High PS concentrations have been described in several studies as a major constituent of exo-

somes (28, 29). In oligodendrocytes, nSMase2-mediated ceramide production was the driver of exosome formation. When these cells were treated with GW4869, an inhibitor of nSMase2 that binds at the PS-binding site of the enzyme, there was a significant reduction in exosome release (30). We therefore speculate that ceramide-mediated exosome formation occurs through the novel PS-mediated allosteric activation model that we describe in our study. This mechanism could be used to modulate exosome release in pathophysiological conditions such as Alzheimer's disease, wherein amyloid β-peptide (Aβ) levels are dysregulated in the brain. It was shown that release of neural exosomes that bind to Aβ peptides could be reduced when the murine microglial cell line BV-2 was treated with nSMase2 siRNA (31).

Several studies on membrane proteins with multiple domains such as receptor tyrosine kinases have described a role for linkers in their function, typically by aiding homo- or heterodimerization or localization (32–34). To date, nSMase2 has not been shown to function as a dimer, nor has the JX region of nSMase2 been shown to play a role in nSMase2 localization, thus making the role of the JX region in enzyme activation unique. This proposed role for the JX region might provide an important example to understand the mechanism of other enzymes in the SMase family. For example, X-ray crystal structures of acid SMase have been solved in both enzymatically active as well as inactive states, but how this enzyme changes conformations from inactive to active still remains unknown because of a lack of conformational dynamic information (35). Interestingly, deletion of the membrane-inserted saposin domain and the linker connecting it to the CAT domain results in loss of acid SMase activity (35). Our study raises the possibility that a similar interdomain relay system might exist in the acid SMase, even though it belongs to a distinct family of SMases.

Many questions still remain unanswered about regulation of nSMase2. For example, although we know that NTD binds PA in the HS1 region leading to enzyme activation with a higher K_m and lower V_{max} (as compared to PS activation of nSMase2), we do not yet understand the mechanism by which PA binding leads to nSMase2 activation. The difference in kinetic parameters suggests that nSMase2 adopts a different active conformation, implying that JX may exist in more than one structural arrangement depending on the input signal. We also speculate that nSMase2 binds to either PA and/or PS in response to specific upstream signals and effect specific downstream outcomes, thus also acting as an important mediator within phospholipid driven pathways.

Several reports on the cellular mechanisms of nSMase2 have placed it in critical junctures in pathways of apoptosis, cell differentiation, and exosome release (36, 37). In light of these functions, various studies over the last two decades have proposed nSMase2 as a major therapeutic target, Because of its role in pathologies such as cancer, inflammation, hypertension, and Alzheimer's disease (8, 38, 39). Thus, understanding the mechanism of nSMase2 activation from the perspective of an allosteric site would potentially be very important in designing inhibitors that are specific to one isoform of nSMase.

Experimental procedures

Protein expression and purification

Overexpression of human nSMase2 CAT and JX-CAT was performed using BL21 (DE3) RIPL cells grown at 37 °C to an OD of 1–1.5 and then cooled to 15 °C. The cells were then induced with 400 μM isopropyl-β-D-1-thigalactopyranoside for 48 h. The cells were then harvested and lysed by sonication with lysis buffer (50 mM sodium phosphate, pH 7.5, 60 mM imidazole, 500 mM NaCl, 5% (v/v) glycerol, and 2 mM β-mercaptoethanol (β-ME)). Cell lysates were then centrifuged and applied to a HisTrap FF column (GE Healthcare) and washed with five column volumes of the lysis buffer. The protein constructs were then eluted using the elution buffer (50 mM sodium phosphate, pH 7.0, 300 mM imidazole, 50 mM NaCl, 5% glycerol (v/v), 10 mM DTT, and 10 mM β-ME). The eluted fraction was incubated at 4 °C with ULP-1 (ubiquitin-like specific protease-1) to cleave the His-SUMO tag and then applied to a size exclusion column (GE Healthcare Superdex 200 Hi-Load 26/60) equilibrated with buffer (20 mM Bis-Tris (pH 6.5), 100 mM NaCl, 10 mM β-ME, and 2 mM DTT). Pooled nSMase2 fractions were concentrated to 10 mg/ml, flash frozen, and stored at −80 °C.

Membrane yeast two-hybrid system

A split ubiquitin-based membrane yeast two-hybrid DUALHunter system (Dualsystems Biotech) was used to study interdomain interactions. Bait was generated using either the nSMase2 CAT or JX-CAT sequence (119–655 Δ175–339 or 85–655 Δ175–339) cloned in the pDHB1 vector containing an OST4 membrane anchor and the C terminus of ubiquitin. This vector contains a Leu2 auxotrophic marker that allows for the selection of positive clones in selective dropout −Leu plates. The prey was generated by cloning the NTD (amino acids 1–84) or NTD-JX (amino acids 1–104 and 1–118) region of nSMase2 into the pPR3N vector. This vector contains NUb and the Trp1 selective marker. The bait and prey were transformed into NMY51 cells via the lithium acetate method, and the cells were grown on selective dropout −Leu −Trp plates. Quantitative assessment of interactions was confirmed by using the β-gal assay following cell lysis with Vortex Genie with TurboMix attachment.

Western blotting analysis

NMY51 cells containing bait and prey were grown at 30 °C for 24 h, pelleted, washed with PBS buffer, and lysed using Vortex Genie with TurboMix attachment. Protein amounts were quantitated using Bradford assay using Bradford reagent (Thermo Fisher). Equal amounts of protein samples were separated on SDS-PAGE using the Bio-Rad Criterion system. Separated proteins were then transferred onto nitrocellulose membranes (Bio-Rad) and blocked with 5% nonfat milk in PBS-T buffer for 1 h at room temperature. Primary antibodies (1:1000 dilution) were then added and incubated at 4 °C overnight. The membranes were washed three times with PBS-T buffer and incubated with respective secondary antibodies (1:5000 dilution) for 1 h at room temperature. The membrane was then washed five times with PBS-T buffer and developed using chemiluminescence with the ECL substrate (Pierce).

Small angle X-ray scattering

SAXS data were collected at the 16-ID Beamline (National Synchrotron Light Source II, Brookhaven National Laboratories). Protein samples at various concentrations with their matching buffer samples were incubated with and without 1 mM 06:0 PS (Avanti) for 5 min before data collection. They were then loaded on to the sample chamber and checked for protein concentration or aggregation effects. Scattering from buffer samples were subtracted to generate scattering curves of protein alone. Guinier plots were analyzed using PRIMUS and used to calculate the radius of gyration, R_g. Pair distribution functions $P(r)$ were calculated using the GNOM package (40).

Hydrogen–deuterium exchange MS

HDX experiments were performed with or without liposomes (30 mol% SM, 10 mol% DOPS, 30 mol% cholesterol, and 30 mol% DOPC) in a total reaction volume of 50 μl with a final protein concentration (CAT or JX-CAT) of 600 nM. Deuterium incorporation was initiated by the addition of 40 μl of deuterium oxide buffer (35 mM Bis-Tris, pH 6.5, 150 mM NaCl, and 99% (v/v) deuterium oxide). The constructs were allowed to exchange over three time courses: 3, 30, and 300 s at 23 °C. Exchange was terminated by the addition of 20 μl of ice-cold quench buffer (3% formic acid, 2 M guanidine HCl), and samples were immediately frozen in liquid nitrogen.

HDX experiments performed comparing the deuterium incorporation of JX-CAT and CAT were performed as above with the addition of a total of 45 μl of D_2O buffer to the protein sample starting the reaction (10 mM HEPES, pH 7.5, 100 mM NaCl, and 99% (v/v) deuterium oxide). Deuterium exchange was allowed to occur over four time courses: 3, 30, 300, and 3000 s. Termination of exchange was performed as above.

HDX-MS experiments were carried out as described previously (41, 42). In brief, samples were quickly thawed and injected onto an ultra-performance LC system (Dionex Ultimate 3000 RSLCnano system coupled to a leap technologies PAL RTC) at 2 °C. The samples were subjected to two immobilized pepsin columns (Applied Biosystems, Poroszyme, 2-3131-00) at 10 and 2 °C, respectively, at a flow of 200 μl/min for 3 min. Peptides were subsequently collected and desalted on a VanGuard precolumn Trap column (Waters) and were eluted onto an Acquity 1.7 μM particle, 100 × 1 mm^2 C18 ultra-performance LC column (Waters). Separation and elution of peptides from the analytical column was achieved using a gradient ranging from 3 to 70% mobile phase B (buffer A: 0.1% formic acid, LC/MS grade; buffer B: 100% acetonitrile, LC/MS grade) over 16 min. Mass spectrometry analyses were performed using an Impact II TOF (Bruker) with an electrospray ionization source operated at a temperature of 200 °C and a spray voltage of 4.5 kV, and data were acquired over a range of 150–2200 m/z. Peptides were identified using a data-dependent acquisition approach. MS/MS experiments were performed (0.5-s precursor scan from 150 to 2000 m/z and twelve 0.25-s fragment scans from 150 to 2000 m/z), and the MS/MS data were analyzed against a database consisting of all proteins previously analyzed in-house, as well as known contaminants using the PEAKS7 software. The false discovery rate was set to 1%.

Levels of deuterium incorporation were calculated using the HDExaminer Software (Sierra Analytics), and data from each individual peptide were inspected for correct charge state, quality of spectra, and the presence of overlapping peptides. Levels of deuteration were computed by HDExaminer using the centroid of the isotopic cluster corresponding to each peptide at each time point. The deuteration levels calculated were presented as relative levels of deuterium incorporation, and back exchange was controlled for by taking into account the total level of deuterium present in the samples (74.8%). The data were further analyzed and curated using Excel, and changes in deuteration levels above 7% and 0.4 Da with a paired t test value of $p < 0.01$ were deemed to be significant.

SMase activity assay

SMase activity assays were performed using SM that was labeled in the choline headgroup with ^{14}C. Porcine brain SM (Avanti Polar Lipids) and PS (Avanti Polar Lipids) were added in required amounts along with trace amounts of radiolabeled SM and dried under N_2 gas. The mixtures were then resuspended in assay buffer containing 0.1% Triton X-100 (Research Products International). The final reaction mix contained 200 μl of lipids and nSMase2 in 100 mM Tris (pH 7.5), 50 mM $MgCl_2$, 5 mM β-ME, and 5 mM DTT. The reaction mix was incubated at 37 °C for 1 h and quenched using 2:1 $CHCl_3$/MeOH to perform a modified Bligh–Dyer extraction. The aqueous phase containing the ^{14}C-labeled and released phosphocholine headgroup was transferred to scintillation vials and quantitated using the Beckman LS 6500 scintillation counter.

Hydroxyurea sensitivity assay

JK9-3d, JK9-3d isc1Δ or JK9-3d isc1Δ cells transformed with various constructs of human nSMase2 were grown overnight at 30 °C using standard YPD medium. The cells were then subcultured at an OD of 0.1 the following morning. The cells were then pelleted and washed twice with ultrapure water once the OD reached 0.3. They were then serially diluted and spotted onto YPD agar plates and YPD agar plates containing 10 mg/ml hydroxyurea (Sigma). The plates were incubated at 30 °C for 72 h.

Protein fold recognition using Phyre2

nSMase2 WT construct was used as the input parameter for prediction of protein secondary structure and fold using the Phyre2 webserver using the "intensive" modeling mode. Next, the same procedure was repeated after making a construct containing D32A, R33A, L34A, K45AR46AQ47AR48A, W85A, P87A, R92AR93A, Y97A, N142AN143A, and L144A mutations. The results were then compared visually.

Thermal shift assay

Thermal stability of CAT WT, JX-CAT WT, and their mutants CAT D430A, CAT N142AN143A, CAT L144A, JX-CAT W85A, JX-CAT R92AR93A, and JX-CAT Y97A was checked by mixing 5 μM of each construct with 1× SYPRO orange dye to bring the total volume up to 50 μl in a 96-well Fast RT-PCR plate. Buffer for all constructs were kept the same (20 mM Bis-Tris, 150 mM NaCl). The temperature range spanned

ASBMB

from 25 to 95 °C at the rate of increase of 1 °C/min in the Applied Biosystems 7500 Fast Real Time PCR machine. The data were analyzed in the 7500 software to obtain T_m from $n = 4$ and plotted as means ± S.D.

CD

CD spectrum measurements were taken using a Jasco spectrometer. nSMase2 samples were dialyzed into 20 mM sodium phosphate buffer, pH 7.5, and diluted to ~5 μM. All spectra were recorded from 190 to 240 nm at 1-nm intervals using a 0.1-cm-pathlength cuvette. Each sample was cumulatively scanned four times and plotted as an average of all four reads. Composition of α-helices and β-sheets was calculated using the K2D3 server (43).

Author contributions—P. S., M. V. A., and Y. A. H. conceptualization; P. S., R. M. H., R. M., and D. J. H. data curation; P. S., R. M. H., D. J. H., and J. E. B. formal analysis; P. S. and Y. A. H. investigation; P. S. visualization; P. S., R. M. H., R. M., and J. E. B. methodology; P. S. writing-original draft; P. S., M. V. A., M. G.-D., J. E. B., and Y. A. H. writing-review and editing; M. G.-D., J. E. B., and Y. A. H. resources; M. G.-D., J. E. B., and Y. A. H. supervision; M. G.-D. validation; J. E. B. project administration; Y. A. H. funding acquisition.

Acknowledgments—We also thank Dr. Lin Yang and Dr. Shirish Chodankar at Brookhaven National Lab National Synchrotron Light Source II for their help with SAXS data collection and data processing. The LiX Beamline is part of the Life Science Biomedical Technology Research resource, jointly supported by the NIGMS, National Institutes of Health under Grant P41 GM111244 and by the Department of Energy Office of Biological and Environmental Research under Grant KP1605010, with additional support from National Institutes of Health Grant S10 OD012331. National Synchrotron Light Source II is a U.S. Department of Energy Office of Science User Facility operated for the Department of Energy Office of Science by Brookhaven National Laboratory under Contract DE-SC0012704. We would also like to thank Dr. Erwin London for help with circular dichroism data collection and analysis. We thank Dr. Lina Marie Obeid and Dr. Chiara Luberto for helpful discussions and feedback.

References

1. Obeid, L. M., and Hannun, Y. A. (1995) Ceramide: a stress signal and mediator of growth suppression and apoptosis. *J. Cell. Biochem.* **58,** 191–198 CrossRef Medline
2. Hannun, Y. A., and Obeid, L. M. (2008) Principles of bioactive lipid signalling: lessons from sphingolipids. *Nat. Rev. Mol. Cell Biol.* **9,** 139–150 CrossRef Medline
3. Kosaka, N., Iguchi, H., Hagiwara, K., Yoshioka, Y., Takeshita, F., and Ochiya, T. (2013) Neutral sphingomyelinase 2 (nSMase2)-dependent exosomal transfer of angiogenic microRNAs regulate cancer cell metastasis. *J. Biol. Chem.* **288,** 10849–10859 CrossRef Medline
4. Kim, W. J., Okimoto, R. A., Purton, L. E., Goodwin, M., Haserlat, S. M., Dayyani, F., Sweetser, D. A., McClatchey, A. I., Bernard, O. A., Look, A. T., Bell, D. W., Scadden, D. T., and Haber, D. A. (2008) Mutations in the neutral sphingomyelinase gene SMPD3 implicate the ceramide pathway in human leukemias. *Blood* **111,** 4716–4722 CrossRef Medline
5. Revill, K., Wang, T., Lachenmayer, A., Kojima, K., Harrington, A., Li, J., Hoshida, Y., Llovet, J. M., and Powers, S. (2013) Genome-wide methylation analysis and epigenetic unmasking identify tumor suppressor genes in hepatocellular carcinoma. *Gastroenterology* **145,** 1424–1435.e1–25 CrossRef Medline
6. Shamseddine, A. A., Airola, M. V., and Hannun, Y. A. (2015) Roles and regulation of neutral sphingomyelinase-2 in cellular and pathological processes. *Adv. Biol. Regul.* **57,** 24–41 CrossRef Medline
7. Chaube, R., Kallakunta, V. M., Espey, M. G., McLarty, R., Faccenda, A., Ananvoranich, S., and Mutus, B. (2012) Endoplasmic reticulum stress-mediated inhibition of NSMase2 elevates plasma membrane cholesterol and attenuates NO production in endothelial cells. *Biochim. Biophys. Acta* **1821,** 313–323 CrossRef Medline
8. Cogolludo, A., Moreno, L., Frazziano, G., Moral-Sanz, J., Menendez, C., Castañeda, J., González, C., Villamor, E., and Perez-Vizcaino, F. (2009) Activation of neutral sphingomyelinase is involved in acute hypoxic pulmonary vasoconstriction. *Cardiovasc. Res.* **82,** 296–302 Medline
9. Sagy-Bross, C., Hadad, N., and Levy, R. (2013) Cytosolic phospholipase A2α upregulation mediates apoptotic neuronal death induced by aggregated amyloid-β peptide1–42. *Neurochem. Int.* **63,** 541–550 CrossRef Medline
10. Wheeler, D., Knapp, E., Bandaru, V. V., Wang, Y., Knorr, D., Poirier, C., Mattson, M. P., Geiger, J. D., and Haughey, N. J. (2009) Tumor necrosis factor-α–induced neutral sphingomyelinase-2 modulates synaptic plasticity by controlling the membrane insertion of NMDA receptors. *J. Neurochem.* **109,** 1237–1249 CrossRef Medline
11. Kong, J. N., He, Q., Wang, G., Dasgupta, S., Dinkins, M. B., Zhu, G., Kim, A., Spassieva, S., and Bieberich, E. (2015) Guggulsterone and bexarotene induce secretion of exosome-associated breast cancer resistance protein and reduce doxorubicin resistance in MDA-MB-231 cells. *Int. J. Cancer* **137,** 1610–1620 CrossRef Medline
12. Singh, R., Pochampally, R., Watabe, K., Lu, Z., and Mo, Y. Y. (2014) Exosome-mediated transfer of miR-10b promotes cell invasion in breast cancer. *Mol. Cancer* **13,** 256 CrossRef Medline
13. Shanbhogue, P., and Hannun, Y. A. (2018) Exploring the therapeutic landscape of sphingomyelinases. *Handb. Exp. Pharmacol.*, in press CrossRef Medline
14. Guo, B. B., Bellingham, S. A., and Hill, A. F. (2016) Stimulating the release of exosomes increases the intercellular transfer of prions. *J. Biol. Chem.* **291,** 5128–5137 CrossRef Medline
15. Kolmakova, A., Kwiterovich, P., Virgil, D., Alaupovic, P., Knight-Gibson, C., Martin, S. F., and Chatterjee, S. (2004) Apolipoprotein C-I induces apoptosis in human aortic smooth muscle cells via recruiting neutral sphingomyelinase. *Arterioscler. Thromb. Vasc. Biol.* **24,** 264–269 CrossRef Medline
16. Shamseddine, A. A., Clarke, C. J., Carroll, B., Airola, M. V., Mohammed, S., Rella, A., Obeid, L. M., and Hannun, Y. A. (2015) p53-dependent upregulation of neutral sphingomyelinase-2: role in doxorubicin-induced growth arrest. *Cell Death Dis.* **6,** e1947 CrossRef Medline
17. Milhas, D., Clarke, C. J., Idkowiak-Baldys, J., Canals, D., and Hannun, Y. A. (2010) Anterograde and retrograde transport of neutral sphingomyelinase-2 between the Golgi and the plasma membrane. *Biochim. Biophys. Acta* **1801,** 1361–1374 CrossRef Medline
18. Wu, B. X., Clarke, C. J., Matmati, N., Montefusco, D., Bartke, N., and Hannun, Y. A. (2011) Identification of novel anionic phospholipid binding domains in neutral sphingomyelinase 2 with selective binding preference. *J. Biol. Chem.* **286,** 22362–22371 CrossRef Medline
19. Filosto, S., Fry, W., Knowlton, A. A., and Goldkorn, T. (2010) Neutral sphingomyelinase 2 (nSMase2) is a phosphoprotein regulated by calcineurin (PP2B). *J. Biol. Chem.* **285,** 10213–10222 CrossRef Medline
20. Airola, M. V., Shanbhogue, P., Shamseddine, A. A., Guja, K. E., Senkal, C. E., Maini, R., Bartke, N., Wu, B. X., Obeid, L. M., Garcia-Diaz, M., and Hannun, Y. A. (2017) Structure of human nSMase2 reveals an interdomain allosteric activation mechanism for ceramide generation. *Proc. Natl. Acad. Sci. U.S.A.* **114,** E5549–E5558 CrossRef Medline
21. Stagljar, I., Korostensky, C., Johnsson, N., and te Heesen, S. (1998) A genetic system based on split-ubiquitin for the analysis of interactions between membrane proteins *in vivo*. *Proc. Natl. Acad. Sci. U.S.A.* **95,** 5187–5192 CrossRef Medline
22. Tani, M., and Hannun, Y. A. (2007) Analysis of membrane topology of neutral sphingomyelinase 2. *FEBS Lett.* **581,** 1323–1328 CrossRef Medline

23. Kelley, L. A., and Sternberg, M. J. (2009) Protein structure prediction on the Web: a case study using the Phyre server. *Nat. Protoc.* **4,** 363–371 CrossRef Medline
24. de Andrade, S. A., Pedrosa, M. F., de Andrade, R. M., Oliva, M. L., van den Berg, C. W., and Tambourgi, D. V. (2005) Conformational changes of Loxosceles venom sphingomyelinases monitored by circular dichroism. *Biochem. Biophys. Res. Commun.* **327,** 117–123 CrossRef Medline
25. Clarke, C. J., Truong, T. G., and Hannun, Y. A. (2007) Role for neutral sphingomyelinase-2 in tumor necrosis factor α-stimulated expression of vascular cell adhesion molecule-1 (VCAM) and intercellular adhesion molecule-1 (ICAM) in lung epithelial cells: p38 MAPK is an upstream regulator of nSMase2. *J. Biol. Chem.* **282,** 1384–1396 CrossRef Medline
26. Wang, G., Dinkins, M., He, Q., Zhu, G., Poirier, C., Campbell, A., Mayer-Proschel, M., and Bieberich, E. (2012) Astrocytes secrete exosomes enriched with proapoptotic ceramide and prostate apoptosis response 4 (PAR-4): potential mechanism of apoptosis induction in Alzheimer disease (AD). *J. Biol. Chem.* **287,** 21384–21395 CrossRef Medline
27. Yeung, T., Heit, B., Dubuisson, J. F., Fairn, G. D., Chiu, B., Inman, R., Kapus, A., Swanson, M., and Grinstein, S. (2009) Contribution of phosphatidylserine to membrane surface charge and protein targeting during phagosome maturation. *J. Cell Biol.* **185,** 917–928 CrossRef Medline
28. Fairn, G. D., Schieber, N. L., Ariotti, N., Murphy, S., Kuerschner, L., Webb, R. I., Grinstein, S., and Parton, R. G. (2011) High-resolution mapping reveals topologically distinct cellular pools of phosphatidylserine. *J. Cell Biol.* **194,** 257–275 CrossRef Medline
29. Laulagnier, K., Motta, C., Hamdi, S., Roy, S., Fauvelle, F., Pageaux, J. F., Kobayashi, T., Salles, J. P., Perret, B., Bonnerot, C., and Record, M. (2004) Mast cell- and dendritic cell-derived exosomes display a specific lipid composition and an unusual membrane organization. *Biochem. J.* **380,** 161–171 CrossRef Medline
30. Trajkovic, K., Hsu, C., Chiantia, S., Rajendran, L., Wenzel, D., Wieland, F., Schwille, P., Brügger, B., and Simons, M. (2008) Ceramide triggers budding of exosome vesicles into multivesicular endosomes. *Science* **319,** 1244–1247 CrossRef Medline
31. Yuyama, K., Sun, H., Mitsutake, S., and Igarashi, Y. (2012) Sphingolipid-modulated exosome secretion promotes clearance of amyloid-β by microglia. *J. Biol. Chem.* **287,** 10977–10989 CrossRef Medline
32. Jura, N., Endres, N. F., Engel, K., Deindl, S., Das, R., Lamers, M. H., Wemmer, D. E., Zhang, X., and Kuriyan, J. (2009) Mechanism for activation of the EGF receptor catalytic domain by the juxtamembrane segment. *Cell* **137,** 1293–1307 CrossRef Medline
33. Matsuda, I., and Mishina, M. (2000) Identification of a juxtamembrane segment of the glutamate receptor delta2 subunit required for the plasma membrane localization. *Biochem. Biophys. Res. Commun.* **275,** 565–571 CrossRef Medline
34. Lu, B., Kiessling, V., Tamm, L. K., and Cafiso, D. S. (2014) The juxtamembrane linker of full-length synaptotagmin 1 controls oligomerization and calcium-dependent membrane binding. *J. Biol. Chem.* **289,** 22161–22171 CrossRef Medline
35. Gorelik, A., Illes, K., Heinz, L. X., Superti-Furga, G., and Nagar, B. (2016) Crystal structure of mammalian acid sphingomyelinase. *Nat. Commun.* **7,** 12196 CrossRef Medline
36. Levy, M., Castillo, S. S., and Goldkorn, T. (2006) nSMase2 activation and trafficking are modulated by oxidative stress to induce apoptosis. *Biochem. Biophys. Res. Commun.* **344,** 900–905 CrossRef Medline
37. Kim, M. Y., Linardic, C., Obeid, L., and Hannun, Y. (1991) Identification of sphingomyelin turnover as an effector mechanism for the action of tumor necrosis factor α and gamma-interferon. Specific role in cell differentiation. *J. Biol. Chem.* **266,** 484–489 Medline
38. Horres, C. R., and Hannun, Y. A. (2012) The roles of neutral sphingomyelinases in neurological pathologies. *Neurochem Res* **37,** 1137–1149 CrossRef Medline
39. Jana, A., and Pahan, K. (2010) Fibrillar amyloid-β–activated human astroglia kill primary human neurons via neutral sphingomyelinase: implications for Alzheimer's disease. *J. Neurosci.* **30,** 12676–12689 CrossRef Medline
40. Svergun, D. I. (1992) Determination of the regularization parameter in indirect-transform methods using perceptual criteria. *J. Appl. Crystallogr.* **25,** 495–503 CrossRef
41. Dornan, G. L., Dalwadi, U., Hamelin, D. J., Hoffmann, R. M., Yip, C. K., and Burke, J. E. (2018) Probing the architecture, dynamics, and inhibition of the PI4KIIIα/TTC7/FAM126 complex. *J. Mol. Biol.* **430,** 3129–3142 CrossRef Medline
42. Lucic, I., Rathinaswamy, M. K., Truebestein, L., Hamelin, D. J., Burke, J. E., and Leonard, T. A. (2018) Conformational sampling of membranes by Akt controls its activation and inactivation. *Proc. Natl. Acad. Sci. U.S.A.* **115,** E3940–E3949 CrossRef Medline
43. Louis-Jeune, C., Andrade-Navarro, M. A., and Perez-Iratxeta, C. (2012) Prediction of protein secondary structure from circular dichroism using theoretically derived spectra. *Proteins* **80,** 374–381 CrossRef Medline